

## External bremsstrahlung spectra excited by $^{204}\text{Tl}$ $\beta$ particles in thick targets

M. S. Powar, Salim Ahmad, and M. Singh

Nuclear Science Laboratories, Department of Physics, Punjabi University, Patiala 147 002, India

(Received 24 July 1979)

Spectral distributions of bremsstrahlung produced by  $^{204}\text{Tl}$   $\beta$  particles in thick targets of Perspex, aluminum, copper, tin, and lead have been measured in a sandwich geometry. The contributions of internal bremsstrahlung produced along with the  $\beta$  particles have been determined by magnetic field deflection as well as the  $Z = 0$  extrapolation method. Experimental results agree with Bethe-Heitler Born-approximation theory, corrected for Coulomb-field effects for low- and medium- $Z$  targets, but show 25% positive deviation for high- $Z$  targets. Again it is found that the bremsstrahlung produced in low- $Z$  targets like Perspex is comparable with internal bremsstrahlung, and the corrections for its contribution to measurements by earlier workers can lead to large uncertainties.

### I. INTRODUCTION

Interaction of continuous and monoenergetic electrons with matter is always accompanied by a weak electromagnetic radiation called external bremsstrahlung (EB). It is to be distinguished from the internal bremsstrahlung (IB), which is present in all  $\beta$  emitters and arises from the interaction of outgoing  $\beta$  particles with the Coulomb field of the daughter nucleus. Apart from the experimental studies of EB excited by monoenergetic electrons in thin targets, the production of EB in thick targets using soft ( $^{35}\text{S}$ ) and hard ( $^{32}\text{P}$ )  $\beta$  rays has been investigated by a number of workers.<sup>1-6</sup> But there are no reliable measurements in the intermediate- $\beta$  end-point energy region between 0.5 and 1.0 MeV. A survey of the literature on EB measurements shows that investigation of this energy region for this process will be an important contribution to Born-approximation theory.

$^{204}\text{Tl}$  is a  $\beta$  emitter with an end-point energy of 763.47 keV. The only reported study of EB with this emitter is by Sarma *et al.*,<sup>7</sup> who measured the EB spectra with thick targets of various elements and compared their results with the Bethe-Heitler-Elwert theory. In their measurements of EB they have subtracted the contributions of IB by using Perspex absorbers, thus assuming that EB in Perspex is negligibly small. However, it is found that EB in Perspex is of the same order as the IB itself. Therefore these studies involve large errors. Again there appear some basic errors in the calculations of EB from  $^{204}\text{Tl}$  and  $^{91}\text{Y}$  by these workers as the values of EB from  $^{91}\text{Y}$ , with a  $\beta$  end-point energy of 1.5 MeV, are lower for all elements than the corresponding values for  $^{204}\text{Tl}$  with  $\beta$  end-point energy of 763.47 keV. In fact the EB intensity should increase as the square of energy.

We have taken into account the contribution of

IB to EB measurements by first accurately measuring the IB part only using the magnetic-field-deflection method when the EB component is eliminated. These results agree with the values of IB obtained by extrapolating to  $Z = 0$  the measured values of IB plus EB without magnetic field. This allows unambiguous determination of EB components. Details of experimental measurements, theoretical calculations, and their comparison are given below.

### II. EXPERIMENTAL DETAILS

A carrier free source of  $^{204}\text{Tl}$  supplied as thalious sulfate in an aqueous solution of specific activity  $200 \text{ mCi g}^{-1}$  by Bhabha Atomic Research Centre (BARC) Bombay, was prepared on a thin polythene film of  $1.47 \text{ mg cm}^{-2}$  thickness supported on a Perspex ring of an inner diameter of 5.1 cm. The source material was spread uniformly on a circular area 5 mm in diameter with a plain insulin solution. The source strength was determined to be  $53.5 \pm 4.0 \mu\text{Ci}$ .

Figure 1 gives the details of the experimental arrangement. A Geiger-Müller (G.M.) tube shielded with Mumetal cylinder was placed at a distance of 20 cm from the source and at right angles to the poles of an electromagnet to determine the current sufficient to deflect the most energetic of the  $\beta$  particles. The current in the electromagnet was increased and a plot of current vs  $\beta$  count rate was obtained. The value of the current for which the  $\beta$  count rate merged with the background count rate was determined. This ensured deflection of all the  $\beta$  particles emitted by the source. The G.M. tube was then replaced by a  $\gamma$ -counting assembly which consisted of a 7D8 NaI (Tl) detector of 1.75-in. diameter and 2-in. thickness supplied by the Harshaw Company and coupled to a 6292 Dumount photomultiplier and shielded with Mumetal cylinder. The photo-

multiplier assembly was further enclosed in a close iron cylinder with an opening of 5-cm diameter through which the detector could be seen. The pole pieces of the electromagnet were covered with a Perspex sheet of appropriate thickness to avoid production of EB from iron. A 4-cm thickness of lead lined on the inside with an aluminum sheet provided further shielding for the detector, which was also protected from x rays originating in the lead collimator by placing a brass disc in such a manner that the scattering of photons was reduced to a minimum. The detector was coupled to an ND 1100 series multichannel analyzer system for recording the data. A thorough

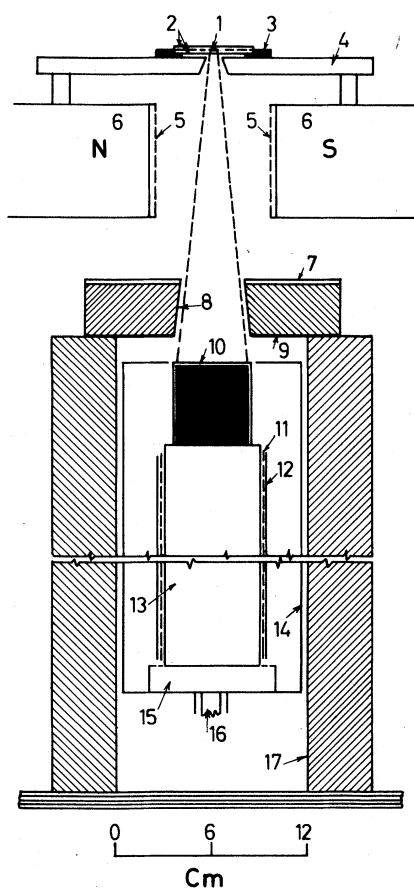


FIG. 1. Experimental apparatus for measurement of IB and EB. 1:  $\beta$  source of  $^{204}\text{Tl}$  on polythene film; 2: targets ( $\beta$  absorbers); 3: Perspex holder; 4: Perspex stand; 5, 6: electromagnet with pole pieces covered with Perspex; 7: Perspex annular disc; 8: lead collimator lined with aluminum on the inside; 9: brass annular plate to absorb lead x rays; 10: NaI (Tl) crystal coupled to photomultiplier; 11: black adhesive tape; 12: Mumetal shielding for photomultiplier tube; 13: photomultiplier; 14: iron cylinder; 15: cathode follower; 16: adjustable support; 17: 4.0-cm-thick lead shielding, inside surface being lined with aluminum.

analysis and comparison of  $^{137}\text{Cs}$   $\gamma$ -ray spectra with and without the magnetic field revealed that there was no distortion arising from the application of the magnetic field.

Targets of lead (308), tin (344.3), copper (366.1), aluminum (318), and Perspex ( $318.6 \text{ mg cm}^{-2}$ ) were prepared so as to stop all the  $\beta$  particles emitted by the source. In a typical measurement the source was sandwiched between two lead targets and placed at distance of 20 cm from the detector along its vertical axis in a Perspex holder of 1-cm thickness and a cut-in cone of sufficient aperture to allow the free passage of EB (and IB) photons originating from the sandwich system. The (IB plus EB) spectra were recorded for sufficiently long intervals of time to obtain good counting statistics (2% at 600 keV for lead). A large number of data runs were taken in a systematic manner to eliminate the effects of electronic drifts, and the average distribution of IB plus EB photons was obtained as shown in Fig. 2. Losses due to the finite dead time of the counting system were corrected automatically by the dead-time compensation mechanism of the multichannel analyzer.

In order to record the IB accompanying the  $\beta$  rays from the source, the targets were removed and magnetic field applied. The data for IB photon distribution along with the background were collected to a good statistical accuracy and are presented in Fig. 2 along with the room background, which was recorded separately. The EB photon distribution for a given target was obtained by subtracting the IB photon distribution from the IB plus EB photon distribution corrected for target self-absorption. Figure 3 shows the distribution of EB photons for targets of lead, tin, copper, aluminum, and Perspex. These distributions were checked by extrapolating the corrected IB plus EB distributions to  $Z = 0$  values from graphs of IB plus EB vs  $Z$  for different values of photon energy. The extrapolated values agreed exceedingly well with the magnetic field values, thus providing a direct check of the experimental procedure adopted here.

### III. CORRECTION TO EB DISTRIBUTION

We reduced spectral distributions of EB photons for various targets to a common window width interval of 10 keV before applying further corrections. In order to convert the spectra recorded by the crystal into those produced in the targets, the spectra of standard  $\gamma$  emitters  $^{57}\text{Co}$ ,  $^{141}\text{Ce}$ ,  $^{203}\text{Hg}$ ,  $^{51}\text{Cr}$ ,  $^{137}\text{Cs}$ , and  $^{54}\text{Mn}$  were recorded in the same geometrical setup. These spectra were then employed to determine energy resolution and photofraction and then backscattered to

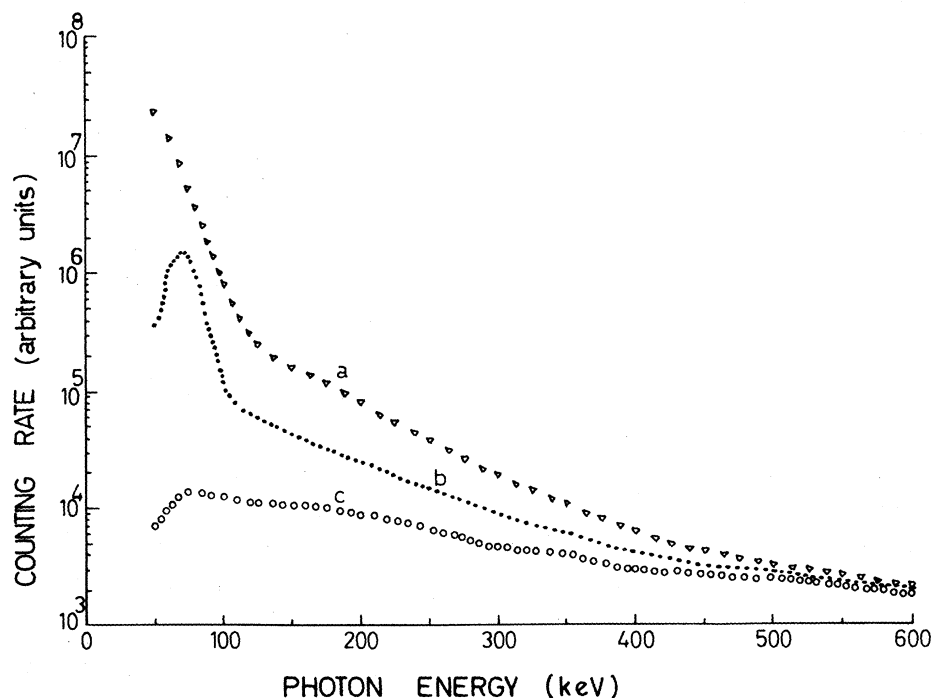


FIG. 2. Experimental pulse height distributions: (a) (IB+EB) distribution corrected for absorption in lead target+background; (b) IB distribution with magnetic field+background; (c) room background distribution.

full energy peak ratios. The EB pulse-height distributions were corrected first for the energy resolution and then the iodine escape peak of the detector system by the procedure used by the authors in their earlier work.<sup>1,8</sup> The combined correction factor due to resolution and the iodine escape peak for EB distribution was found to be significant only at energies below 100 keV; it was 9% at 100 keV and 2% at 350 keV for a lead target and somewhat lower for other targets. Experimentally measured ratios of backscattered to full energy peaks were plotted as a function of energy and used in evaluating the intensities of backscattered peaks for the various targets. In all cases, this contribution was found to be less than 4% and was limited to the energy range 100–200 keV. The EB photon distribution was also corrected for the Compton continuum present in the low-energy region, owing to the higher-energy photons. Spectral data of monoenergetic  $\gamma$  emitters were employed to work out this correction by using a straight-line approximation for Compton continuum distribution. For the lead target this correction was less than 1% at 100 keV and 0.4% at 400 keV, while for other targets the values were still smaller. The various corrections are shown in Fig. 3 for the lead target. The true EB spectra were obtained from the corrected spectral distributions after taking into account the geometrical and intrinsic efficiencies from the data tabulated by Crouthamel<sup>9</sup> for this

detector, and converted into photons per unit energy interval ( $m_0c^2$ ) per  $\beta$  disintegration by dividing the distribution by the window width ( $m_0c^2$  units) and the  $\beta$  strength of the source. These EB photon spectra are shown in Fig. 4 for various targets.

#### IV. ERRORS

The present measurements of EB spectra involved errors which arose mainly from factors determining the response function of the detector. These factors included intrinsic and geometrical detection efficiencies, photofractions, and energy resolution of the detector. Uncertainties in tabulated efficiency are 2–3%, while the experimentally measured photofractions were uncertain by 4% in the entire energy range covered in the present work. This gave an overall error of 5% in the photopeak detection efficiency of the crystal. Errors involved in the corrections for backscattered peak intensities, energy resolution, iodine escape peak, and Compton continuum contribution were negligible as these corrections by themselves were very small, as discussed in Section III. Errors involved in correction for self-absorption in targets depend on uncertainties in attenuation coefficients for  $\gamma$  rays. These are known with an accuracy of 1%.<sup>10</sup> Frequent checks of electronic assembly revealed drifts in energy

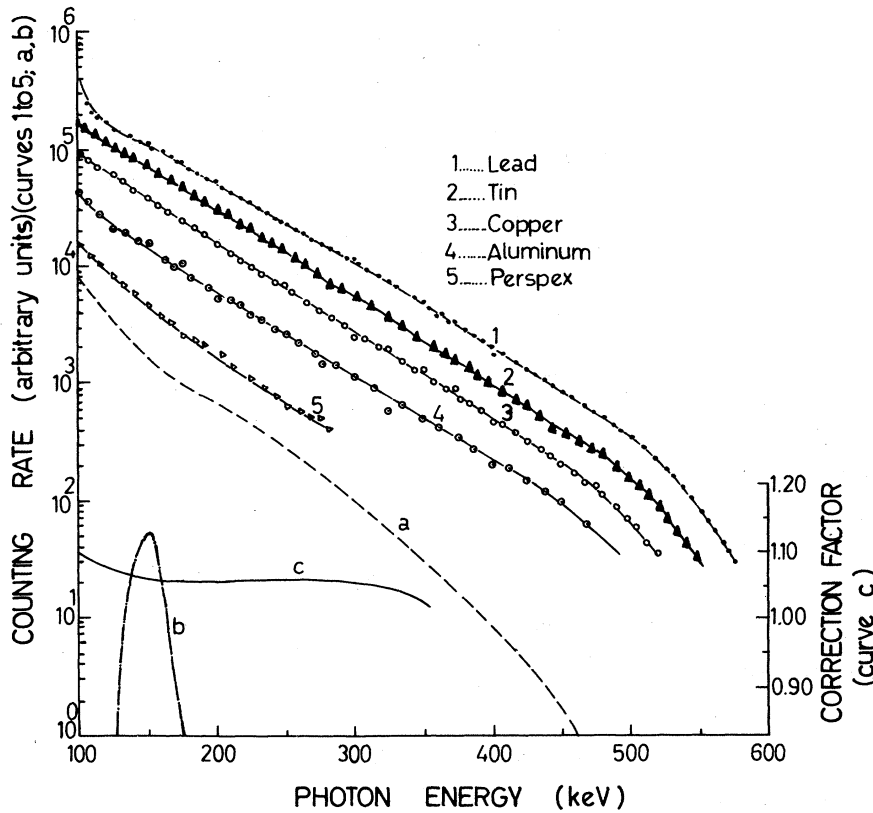


FIG. 3. EB distributions for targets of lead (curve 1), tin (curve 2), copper (curve 3), aluminum (curve 4), and Perspex (curve 5) and corrections for lead EB spectrum. Curve (a) Compton continuum contribution, (b) backscattering peak contribution, and (c) correction factor for iodine K-x-ray escape peak, detector resolution, absorption in air, and aluminum covering can of the detector.

calibration within 1%. Uncertainties due to statistics in recording the data were less than 2% at the highest energy studied for each target. When the various errors were taken into account, the total uncertainty in the measurements was 6%, which was the rms value of the various errors involved. However, this did not include the 8% uncertainty in the measurement of  $\beta$  activity of the source, since the latter affected the EB photon yield and not the photon spectral distribution. As a result, the EB photon spectral distribution for lead was normalized with theory at 150 keV to avoid error due to uncertainty in the  $\beta$  activity of the source, and the other distributions were compared with theory after division by the same factor as that for lead.

## V. THEORY

Bethe and Heitler investigated theoretically the process for the production of external bremsstrahlung which arises from the interaction of the fast-moving electrons with the Coulomb fields of the target nuclei.<sup>11</sup> This theory was developed in the Born approximation independently by Bethe and Heitler, Sauter, and Racah. They calculated the cross section  $\sigma(W_e, k)$  for the production of EB photon of energy between  $k$  and  $k$  plus  $dk$ , integrated over all photon directions by an electron of total energy  $W_e$  (including rest-mass energy  $m_0c^2$ ) when it interacts with the Coulomb field of target nucleus of atomic number  $Z$  and atomic weight  $A$ . The expression for the cross section  $\sigma(W_e, k)$  is given below:

$$\sigma(W_e, k) = \frac{Z^2 \gamma_0^2}{137} \frac{dk}{k} \frac{p}{p_e} \left\{ \frac{4}{3} - 2W_e W \frac{p_e^2 + p^2}{p_e^2 p^2} + \frac{\epsilon_e W}{p_e^3} + \frac{\epsilon W_e}{p^3} - \frac{\epsilon_e \epsilon}{p_e p} \right. \\ \left. + L \left[ \frac{8}{3} \frac{W_e W}{p_e p} + \frac{k^2 (W_e^2 W^2 + p_e^2 p^2)}{p_e^3 p^3} + \frac{k}{2p_e p} \left( \frac{W_e W + p_e^2}{p_e^3} \epsilon_e - \frac{W_e W + p^2}{p^3} \epsilon + \frac{2k W_e W}{p_e^2 p^2} \right) \right] \right\}, \quad (1)$$

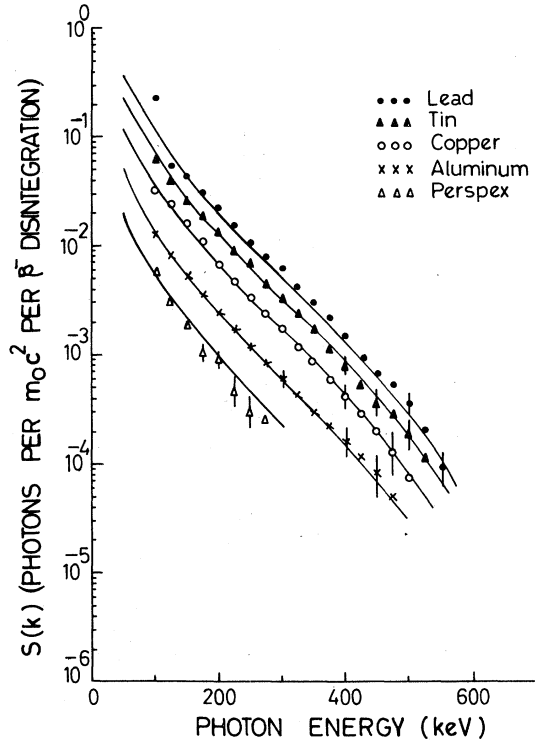


FIG. 4. Experimental EB spectral distributions for the complete absorption of  $^{204}\text{Tl}$   $\beta$  particles in targets of lead, tin, copper, aluminum, and Perspex compared with Bethe-Heitler (Elwert) theory. Errors are the rms values of uncertainties shown at various points for orientation.

where

$$\epsilon_e = \ln \frac{W_e + p_e}{W_e - p_e}, \quad \epsilon = \ln \frac{W + p}{W - p},$$

$$L = 2 \ln \frac{W_e W + p_e p - 1}{k}, \quad \gamma_0 = \frac{e^2}{m_0 c^2} = 2.818 \times 10^{-13} \text{ cm};$$

$W_e$ ,  $p_e$  and  $W, p$  are the initial and final values of electron energy and momentum in units of  $m_0 c^2$  and  $m_0 c$ , respectively, and  $k$  is the photon energy in  $m_0 c^2$  units.

Several correction factors have been suggested to modify the Bethe-Heitler theory to make it more realistic and accurate. Koch and Motz<sup>12</sup> have reviewed the various attempts in this direction. Elwert and Guth have given a correction factor to take into account the effects of Coulomb field towards the low-energy end of the spectrum. This correction factor is known as Elwert factor  $f_E$  and is a function of target atomic number  $Z$ , initial and final values of electron energy and momentum before and after the emission of photon. It is given as

$$f_E = \frac{(W/p)[1 - \exp(-2\pi Z\alpha W_e/p_e)]}{(W_e/p_e)[1 - \exp(-2\pi Z\alpha W/p)]}, \quad (2)$$

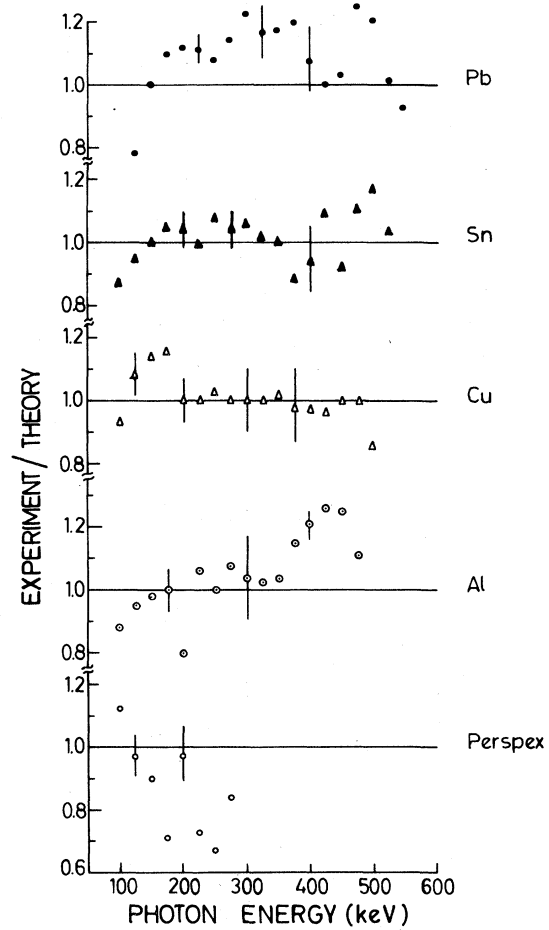


FIG. 5. Shape-factor plots of experiment/theory for EB from various targets. Errors are the rms values of uncertainties shown at various points for orientation.

where  $\alpha$  is a fine-structure constant.

When an electron of energy  $W_e$  is completely absorbed in a target with  $N$  atoms per unit volume, the number of EB photons of energy  $k$  produced is given by  $n(W_e, k)$  such that

$$n(W_e, k) = \int_{1+k}^{W_e} \frac{N\sigma(W, k)f_E}{(-dW/dx)} dW; \quad (3)$$

$-dW/dx$  is the energy loss per unit path length of the target and is given by Knop and Paul.<sup>13</sup>

In the case of  $\beta$  emitter with end-point energy  $W_{\max}$  the bremsstrahlung spectrum is given as  $S(k)$ , the number of photons of energy  $k$  per unit energy interval per  $\beta$  disintegration:

$$S(k) = \frac{\int_{1+k}^{W_{\max}} P(W_e)n(W_e, k)dW_e}{\int_1^{W_{\max}} P(W_e)dW_e}; \quad (4)$$

$P(W_e)dW_e$  is the  $\beta$  spectrum of the isotope under study. Values of  $\sigma(W_e, k)$ ,  $-dW/dx$ , and  $f_E$  were evaluated with the help of a computer for various target materials and  $S(k)$  was evaluated by numerical integration by using the experimental  $\beta$  spectrum for  $^{204}\text{Tl}$  given by Yuasa *et al.*<sup>14</sup> [which agrees closely with the  $\beta$  spectrum obtained from the later (1967) data of Park and Christmas<sup>15</sup>]. It may be mentioned that these distributions ignore the contribution of electron-electron bremsstrahlung and also the effect of the screening of atomic electrons on the nuclear Coulomb field.

## VI. RESULTS AND DISCUSSION

$^{204}\text{Tl}$  is a unique first-forbidden  $\beta$  emitter ( $\Delta J = 2$ , yes), with a half-life of 3.79 yr and maximum  $\beta$  energy<sup>16</sup> of 763.47 keV. There also exists a weak electron-capture branch (2.1%) in it. The presence of  $K$  x rays of  $^{204}\text{Hg}$  (80 keV) contributes to uncertainties in EB measurements below 100 keV with the result that experimental results can be compared with theory above 100 keV only. Figures 4 and 5 compare EB distributions from various targets with Bethe-Heitler-Elwert theory. The errors shown at various points include the statistical uncertainties which increase with the energy, being the difference of two equally important quantities, viz., IB plus EB and IB. The measurements with lead targets extend up to 550 keV and the experimental value is consistently higher than the Bethe-Heitler theory (matched at 150 keV with experiment). Deviations vary from 12% at 200 keV to 25% at 475 keV. In the case of other targets the agreement between experiment and theory is much better. In tin it is within 10% in the entire energy region 100–525 keV, while in copper it is within 5% from 100 to 500 keV, in aluminum it is within 7% from

100 to 475 keV except that there is a weak hump of +25% at 450 keV. In the case of Perspex with an effective atomic number of 5.85, the experimental results are somewhat lower than the theoretical values (–20% at 275 keV).

Direct comparison of present measurements with those of Sarma *et al.*<sup>7</sup> is not possible because they have presented their results in terms of photons per MeV per  $\beta$  disintegration per tin atom for all targets. As mentioned above in Section I, it appears that there is some error in their calculation of EB from  $^{204}\text{Tl}$  and  $^{91}\text{Y}$  because the EB in the latter is lower than in the former, although the end-point energy of  $^{91}\text{Y}$  is higher than that of  $^{204}\text{Tl}$  by a factor of 2.

The present investigations of EB from Perspex, however, reveal that it is of the same order of magnitude as the IB from  $^{204}\text{Tl}$   $\beta$  emitter. The ratio of EB in Perspex to IB varies from 57% at 100 keV to 36% at 275 keV. Thus the assumption that EB from Perspex, or for that matter from other low- $Z$  targets, can be neglected (or corrected for approximately) in the measurements of IB (or EB from other elements) is not correct and is bound to lead to appreciable errors. The present measurements show that there is a reasonably good agreement between experiment and the Elwert corrected Bethe-Heitler theory for EB for low- and medium- $Z$  targets, but there are positive deviations of experiment from theory for high- $Z$  elements like lead ( $Z = 82$ ), for which the values are found to increase with photon energy. The reason for this may be ascribed partly to screening of nuclear charge, which is not taken into account in the calculations. This behavior of the experimental results for  $^{204}\text{Tl}$  with  $E_{\beta}^{\text{max}}$  of 763.47 keV is similar to that of soft- $\beta$  emitter  $^{35}\text{S}$  with  $E_{\beta}^{\text{max}}$  of 167 keV and hard- $\beta$  emitter like  $^{32}\text{P}$  with  $E_{\beta}^{\text{max}}$  of 1710 keV, and it points to the inadequacy of theory for the process of EB production.

<sup>1</sup>Salim Ahmad, M. S. Powar, and M. Singh, *Phys. Rev. A* **19**, 2009 (1979).

<sup>2</sup>R. Prasad Babu, K. Narasimha Murthy, and V. A. Narasimha Murthy, *J. Phys. G* **1**, 273 (1975).

<sup>3</sup>T. S. Mudhole, *Ind. J. Pure Appl. Phys.* **11**, 199 (1973).

<sup>4</sup>C. Bussolati, *Nuovo Cimento* **13**, 909 (1959).

<sup>5</sup>K. Liden and N. Starfelt, *Phys. Rev.* **97**, 419 (1955).

<sup>6</sup>N. Starfelt and N. Svantesson, *Phys. Rev.* **97**, 708 (1955).

<sup>7</sup>K. V. N. Sarma, K. Narasimha Murthy, and V. V. V. Subrahmanyam, *Nucl. Sci. Eng.* **61**, 195 (1976).

<sup>8</sup>M. S. Powar and M. Singh, *J. Phys. G* **2**, 43 (1976).

<sup>9</sup>C. E. Crouthamel, *Applied Gamma Ray Spectrometry* (Pergamon, New York, 1960), p. 321.

<sup>10</sup>J. H. Hubbell, *Natl. Stand. Ref. Data. Ser. Natl. Bur. Stand.* **29** (1969).

<sup>11</sup>For a general review, see R. R. Roy and R. D. Reed, *Interactions of Photons and Leptons with Matter* (Academic, New York, 1968), pp. 139–170.

<sup>12</sup>H. W. Koch and J. W. Motz, *Rev. Mod. Phys.* **31**, 920 (1959).

<sup>13</sup>G. Knop and W. Paul, *Alpha-, Beta-, and Gamma-Ray Spectroscopy*, edited by Kai Siegbahn (North-Holland,

- Amsterdam, 1968), Vol. I, p. 12.
- <sup>14</sup>T. Yuasa, J. Laberrigue-Frolow, and L. Feuvrais, *J. Phys. Radium* 16, 39 (1955).
- <sup>15</sup>J. J. H. Park and P. Christmas, *Can. J. Phys.* 45, 2621 (1967).
- <sup>16</sup>C. M. Lederer and V. S. Shirley (editors), *Table of Isotopes*, 7th ed. (Wiley, New York, 1978), p. 1310.